Myosin VIIa and sans localization at stereocilia upper tip-link density implicates these Usher syndrome proteins in mechanotransduction

M'hamed Grati and Bechara Kachar[1]

Laboratory of Cell Structure and Dynamics, National Institute on Deafness and Other Communication Disorders, National Institutes of Health, Bethesda, MD 20892

Edited by Jonathan G. Seidman, Harvard Medical School, Boston, MA, and approved June 8, 2011 (received for review March 14, 2011)

In the most accepted model for hair cell mechanotransduction, a cluster of myosin motors located at the stereocilia upper tip-link density (UTLD) keeps the tip-link under tension at rest. Both myosin VIIa (MYO7A) and myosin 1c have been implicated in mechanotransduction based on functional studies. However, localization studies are conflicting, leaving open the question of which myosin localizes at the UTLD and generates the tip-link resting tension. Using immunofluorescence, we now show that MYO7A and sans, a MYO7A-interacting protein, cluster at the UTLD. Analysis of the immunofluorescence intensity indicates that eight or more MYO7A molecules are present at each UTLD, consistent with a direct role for MYO7A in maintaining tip-link tension. MYO7A and sans localization at the UTLD is confirmed by transfection of hair cells with GFP-tagged constructs for these proteins. Cotransfection studies in a heterologous system show that MYO7A, sans, and the UTLD protein harmonin-b form a tripartite complex and that each protein is capable of interacting with one another independently. We propose that MYO7A, sans, and harmonin-b form the core components of the UTLD molecular complex. In this complex, MYO7A is likely the motor element that pulls on CDH23 to exert tension on the tip-link.

Stereocilia convert mechanical vibrations into electrical signals via the coordinated interactions of multiple proteins precisely positioned within the mechanotransduction (MET) complex (1–3). The MET complex is built around a tip-link, made of cadherin-23 (CDH23) and protocadherin-15 (4), that connects two adjacent stereocilia in the direction of mechanosensitivity of the hair bundle. A protein-dense plaque or density underlies the stereocilia membrane at each end of the tip-link (5). The upper tip-link insertion density (UTLD) is presumed to contain a cluster of motor proteins that pulls on the tip-link to maintain a resting tension (2, 3). Conversely, when stimulus forces deflect stereocilia and further tense the tip-link, the UTLD presumably slides downward as part of the putative adaptation mechanism that enables the hair cell to maintain optimal dynamic range and sensitivity to stimuli (1, 2, 6).

In the most widely accepted model, myosin 1c (MYO1C) is the tensing or adaptation motor (2). MYO1C has been proposed as the motor based on early immunolocalization (7, 8) and functional studies (9). In contrast, other attempts failed to detect MYO1C concentrated at the predicted UTLD site (10). In support of an alternative hypothesis that myosin VIIa (MYO7A) is the tip-link tensing motor, an early functional study in MYO7A mutant mice showed that MYO7A was essential to keep tip-links under tension at rest (11). In addition, biochemical evidence indicates that MYO7A interacts with harmonin-b (12), a scaffolding protein concentrated at the UTLD (13). However, there are no reports of localization of MYO7A at the UTLD. Therefore, the identity of the tip-link tensing motor and the localization of MYO7A remain open.

Another protein presumed to interact with MYO7A is the scaffolding protein sans (14, 15). MYO7A, sans, harmonin, and CDH23 are all implicated in Usher type I (USH1) syndrome (16), characterized by deafness, vestibular dysfunction, and retinopathy leading to blindness. The localization reported for sans in hair cells are at the basal body (17) and more recently at the stereocilia tips (18). The lack of information on the precise localization of MYO7A and sans in stereocilia makes it difficult to determine whether these proteins are implicated in MET, and to understand their role in USH1 hearing loss. We have now generated antibodies for both MYO7A and sans, and through immunofluorescence we have found that these two proteins are concentrated at the UTLD. (For validation of the specificity of MYO7A and sans antibodies, see Figs. S1 and S2.) We further examined the colocalization of these proteins by coexpressing tagged forms in hair cells and in COS7 cells. Our studies show that MYO7A, sans, and harmonin-b interact with one another independently, and together form the core of the UTLD molecular complex.

Results

MYO7A Localizes to the UTLD. To examine the localization of MYO7A in stereocilia, we labeled adult mouse, rat, and guinea pig vestibular and organ of Corti tissue with two affinity-purified MYO7A polyclonal antibodies (PB205 and PB206) and with a MYO7A monoclonal (sc-74516) antibody. High-magnification confocal images of stereocilia from vestibular (Fig. 1 *A*–*C*) and organ of Corti hair cells (Fig. 1 *F* and *G*, and Fig. S3*A*) show immunofluorescence localization at the position of the UTLD that, by transmission electron microscopy (Fig. 1*D*), appears as an electron-dense plaque (5). The localization of MYO7A is very similar to the previously described (4) localization of CDH23 (Fig. 1 *E* and *J*). In double-labeling experiments using the MYO7A monoclonal antibody and a polyclonal antibody to the UTLD protein harmonin, we observed alignment of the fluorescence puncta (Fig. 1 *K* and *L*). Aside from the fluorescent puncta at the UTLD, a diffuse MYO7A staining is observed throughout the hair-cell cytoplasm (19). This cytoplasmic MYO7A labeling is commonly used to distinguish hair cells from supporting cells. High-magnification images of the cytoplasm show that this diffuse staining is the result of innumerable, diffraction-limited fluorescence puncta (Fig. 1*H*, *Lower*). Close-up views show that the fluorescence intensity of the UTLD puncta (Fig. 1*H*, *Upper*) is considerably higher than that of the cytoplasm (Fig. 1*H*, *Lower*), suggesting that the UTLD contains multiple copies of MYO7A. To quantify the immunofluorescence, we overlaid each fluorescence puncta in the digital images with a 300-nm diameter circular

Author contributions: M.G. and B.K. designed research; M.G. performed research; M.G. and B.K. analyzed data; and M.G. and B.K. wrote the paper.

The authors declare no conflict of interest.

This article is a PNAS Direct Submission.

Freely available online through the PNAS open access option.

[1]To whom correspondence should be addressed. E-mail: kacharb@nidcd.nih.gov.

This article contains supporting information online at www.pnas.org/lookup/suppl/doi:10.1073/pnas.1104161108/-/DCSupplemental.

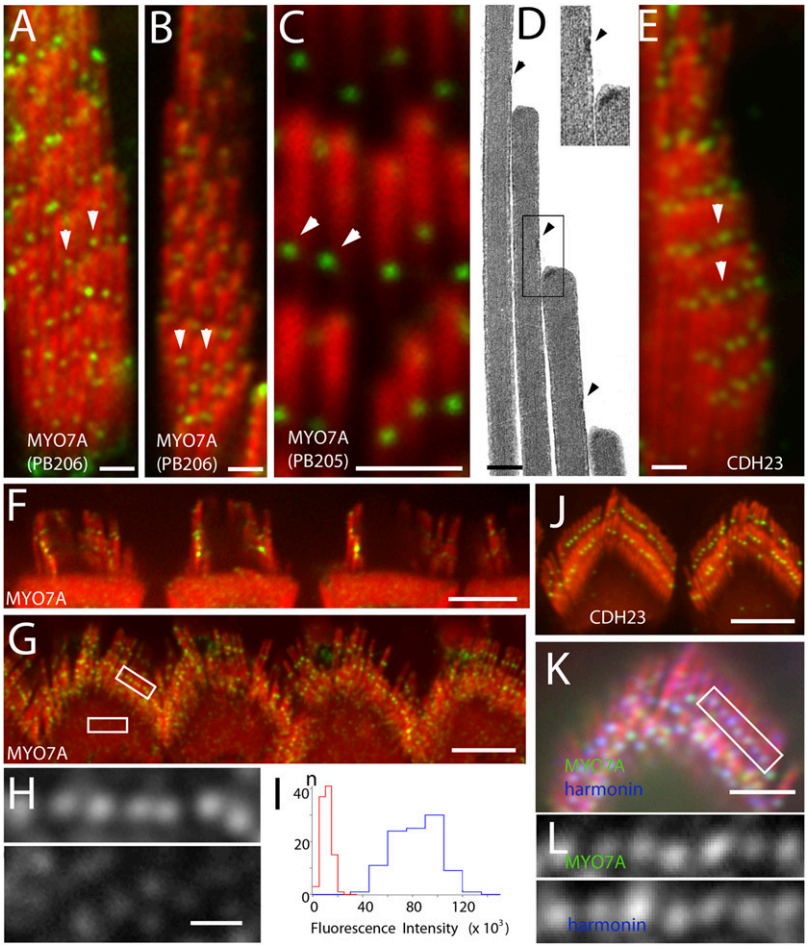

Fig. 1. Localization of MYO7A to the UTLD. (*A–C*) Immunofluorescence confocal images of MYO7A using antibodies PB206 and PB205 in vestibular hair cells of guinea pig showing labeling (green, arrowheads) at the UTLD location. Stereocilia are counterstained in red with rhodamine phalloidin. (*D*) UTLD (arrowheads and *Inset*) in a thin section electron micrograph of a vestibular stereocilia bundle. (*E*) CDH23 labeling in vestibular hair cells is similar to that seen for MYO7A. (*F* and *G*) MYO7A and (*J*) CDH23 labeling at the UTLD in rat outer hair cells. (*H*) Close-up views of the areas indicated by the rectangles show MYO7A fluorescence puncta at the UTLD (*Upper*) and in the cytoplasm (*Lower*). (*I*) Distribution of the MYO7A fluorescence intensity at the UTLD (blue) and cytoplasm (red) puncta. (*K*) Coimmunofluorescence labeling of MYO7A (green) using the sc-74516 antibody and harmonin (blue) in rat outer hair cell. (*L*) Close-up view of green channel (*Upper*) and the blue channel (*Lower*) of the rectangle in *K* show colocalization of the two proteins. [Scale bars: 1 μm (*A–C*, *E*, and *K*), 5 μm (*F*, *G*, and *J*), and 300 nm (*D* and *H*).]

region of interest, and then calculated the integrated relative fluorescence intensity. Although the average fluorescence intensity for the cytoplasmic puncta was $11 \pm 3.9 \times 10^3$ ($n = 100$), the average fluorescence intensity for the UTLD puncta was $83 \pm 18 \times 10^3$ ($n = 100$) for organ of Corti hair cells and $80 \pm 26 \times 10^3$ ($n = 50$) for vestibular hair cells. A histogram of the distribution of these measurements is shown in Fig. 1*I*. Assuming that the cytoplasmic puncta represent staining of soluble monomeric MYO7A (20, 21), it can be inferred that the UTLD contains eight or more MYO7A molecules, depending on how well our antibody had access to all of the MYO7A in the UTLD.

Sans, a MYO7A-Binding Protein, Localizes at the UTLD. To examine whether sans localizes with MYO7A at the UTLD, we used sans-specific antibodies (PB852 and PB906). We observed a pattern of fluorescence labeling (Fig. 2 *A*, *C*, and *D*) very similar to that observed for MYO7A (Fig. 1) and to the previously described (13, 22) localization pattern for the UTLD protein harmonin (Fig. 2 *B* and *E*). We attempted to obtain an approximate estimate of the relative copy numbers of these proteins at the UTLD by calculating for each protein the ratio of the fluorescence intensity at the UTLD to that of the cytoplasmic MYO7A puncta, assuming that it represents the fluorescence intensity that corresponds to a single epitope in our assay (see above). The distribution of the estimated copy numbers for MYO7A, sans, and harmonin is shown in the graph in Fig. 2*F*. Based on the median value of the distribution of fluorescence ratio, the estimated copy number for these proteins was 8:9:23 for MYO7A, sans, and harmonin, respectively. These estimated values are only approximate and could in fact be an underestimation, depending on the epitope accessibility for each protein in the UTLD. No noticeable immunofluorescence was detected around the basal body, as previously reported (17).

GFP-Tagged MYO7A and Sans Target the UTLD. To obtain further evidence on the colocalization of MYO7A and sans at the UTLD, we expressed GFP-tagged forms of these proteins in cultured vestibular hair cells. Fluorescence at the UTLD was observed following transfection with GFP-tagged MYO7A, sans, and harmonin (Fig. 3 *A–C*, respectively). Immunofluorescence labeling for native harmonin also confirms the colocalization with GFP-MYO7A at the UTLD (Fig. 3*D*). The overexpression experiments show particularly robust fluorescence, suggesting that these proteins may be accumulating at the plaques. To

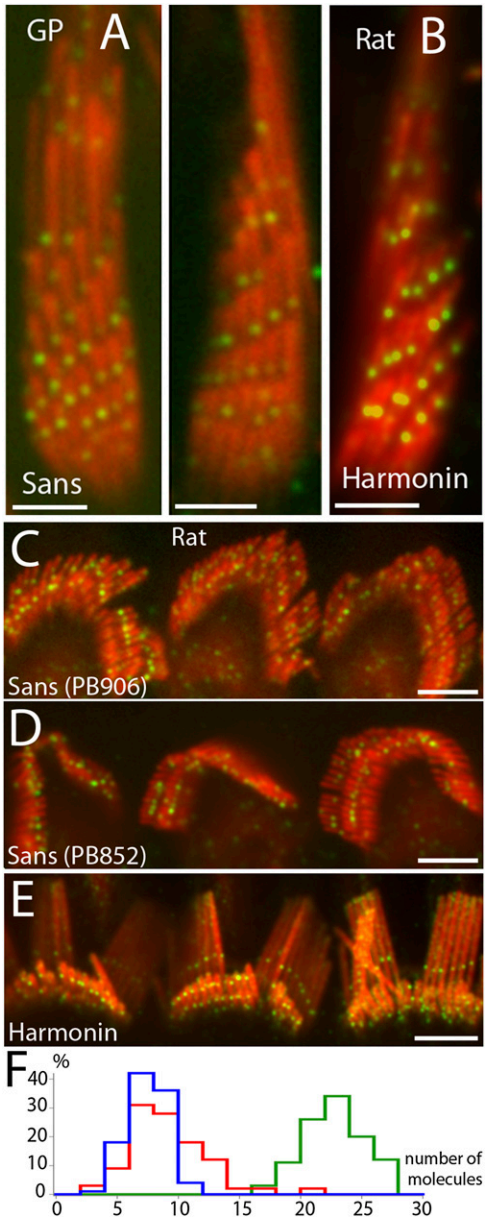

Fig. 2. Localization of sans at the UTLD. (*A*) Immunofluorescence of sans in guinea pig vestibular hair cells using antibody PB852 shows localization (green puncta) corresponding to UTLD location. (*B*) Immunofluorescence of harmonin (green) in rat vestibular hair cells shows localization at the UTLD. (*C* and *D*) Immunofluorescence of sans in rat outer hair cells using antibodies PB906 (*C*) and PB852 (*D*) shows localization (green) in two rows across the tallest and middle stereocilia. (*E*) Harmonin labeling in rat outer hair cells. (*F*) Distribution of the estimated number of MYO7A (blue) sans (red) and harmonin (green) at the UTLD based on the ratio of fluorescence intensity at the UTLD puncta and the intensity of the MYO7A cytoplasmic puncta assuming that it represents the fluorescence intensity that corresponds to a single epitope in our assays (n = 100). [Scale bars: 2 μm (*A* and *B*) and 5 μm (*C*–*E*).]

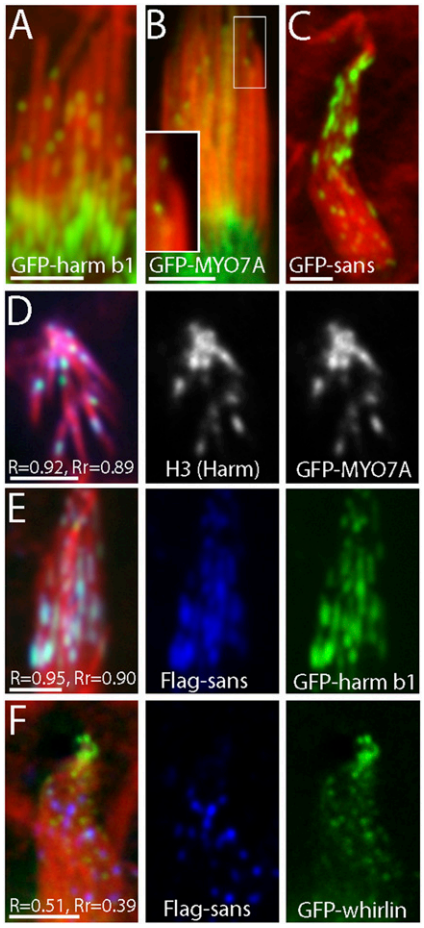

Fig. 3. Harmonin, MYO7A, and sans form clusters and colocalize in plaques along the stereocilia of transfected vestibular hair cells. GFP-harmonin-b (*A*), GFP-MYO7A (*B*), and GFP-sans (*C*) appear in plaques (green) along the side of stereocilia (counterstained in red with rhodamine phalloidin). (*D*) Hair cell expressing GFP-MYO7A (green) and counterstained for harmonin with H3 antibody (blue) show colocalization (R = 0.92, Rr = 0.89) of these proteins. (*E*) Hair cell coexpressing GFP-harmonin-b (green) and Flag-tagged sans (blue) also shows colocalization (R = 0.95, Rr = 0.90) in plaques along the stereocilia. (*F*) Hair cell coexpressing GFP-whirlin (green) and Flag-tagged sans (blue) shows that GFP-whirlin localizes to the stereocilia tips and does not overlap (R = 0.51, Rr = 0.39) with sans localization presumably at the UTLD. (Scale bars: 2 μm.)

evaluate the colocalization quantitatively we calculated the Mander's (R) and Pearson's (Rr) colocalization coefficients (23). The strong colocalization is confirmed by the combined high values for R and Rr for MYO7A and harmonin (Fig. 3*D*) and for sans and harmonin (Fig. 3*E*). Interestingly, cells cotransfected with Flag-tagged sans and GFP-whirlin, a stereocilia scaffolding protein that was previously reported to bind to sans (24), did not show significant colocalization, as demonstrated by the low R and Rr values (Fig. 3*F*). This finding is consistent with the observation that whirlin localizes to stereocilia tips rather than to the UTLD (2).

MYO7A, Sans, and Harmonin Form a Tripartite Complex. Because MYO7A, sans, and harmonin have been shown to interact with each other in biochemical assays (15), we wanted to examine whether they interact in an in vivo heterologous system. We performed single, double, and triple transfections of COS7 cells with tagged MYO7A, sans, and harmonin-b. When GFP-MYO7A was expressed alone (Fig. 4*A*), a diffuse fluorescence was observed throughout the entire COS7 cytoplasm. This lack of colocalization with actin filaments is consistent with a soluble, monomeric MYO7A (20, 21). When GFP-sans was expressed alone (Fig. 4*B*), its pattern of distribution was also diffuse throughout the cytoplasm. However, GFP-harmonin-b expression in COS7 cells leads to the formation of plaques (Fig. 4*C*) associated with actin (12). In triple-transfected COS7 cells, both MYO7A and sans colocalized strongly with the harmonin-b plaques, as indicated by the high Mander's and Pearson's coefficients (Fig. 4*D*).

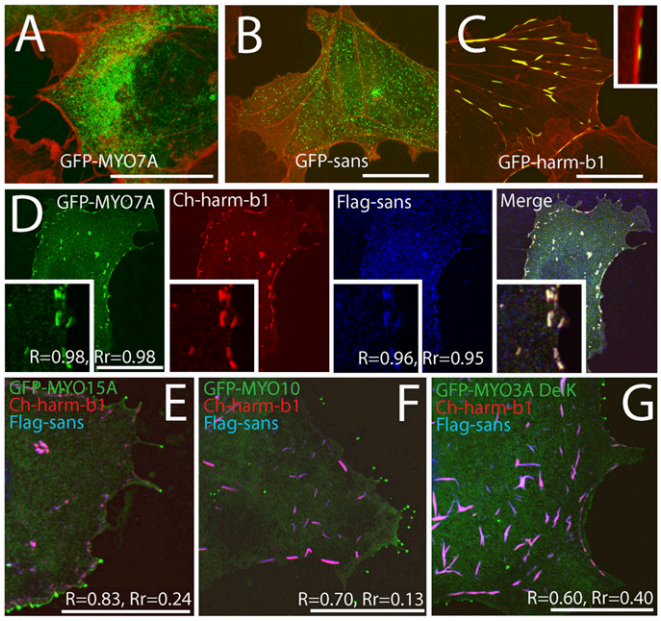

Fig. 4. Tripartite interactions of MYO7A, sans and harmonin in COS7 cells. (*A*) GFP-MYO7A (green) shows a diffuse cytoplasmic distribution with no obvious colocalization with actin (counterstained in red with rhodamine phalloidin). (*B*) In COS7 cells, GFP-sans (green) shows granular distribution in the cytoplasm unrelated to actin bundles (red). (*C*) GFP-harmonin-b (green) form plaques associated with actin (red). (*Inset*) Close-up view. (*D*) COS7 cells expressing GFP-MYO7A (green), Cherry-harmonin-b (red), and Flag-sans (blue) show colocalization of MYO7A and sans in the actin-associated harmonin-b plaques (R = 0.98, Rr = 0.98 and R = 0.96, Rr = 0.95, respectively). COS7 cells expressing Cherry-harmonin-b (red) and Flag-sans (blue) together with GFP-MYO15A (*E*), GFP-MYO10 (*F*), or GFP-MYO3A (*G*) show low Pearson's coefficients (*Rr*) values indicative of weak and random colocalization. Neither harmonin nor sans colocalize with GFP-MYO15A (*E*), GFP-MYO10 (*F*) or GFP-MYO3A (*G*) at filopodia tips. (Scale bars: 5 μm.)

MYO7A has been shown to bind to sans via its MyTH4-FERM domain 1 and to harmonin via its MyTH4-FERM domain 2 (14, 15). Myosin XVa (MYO15A) is another stereocilia myosin that has MyTH4-FERM tail domains (25). To determine whether MYO15A is also capable of interacting with sans and harmonin-b, we coexpressed tagged versions of these proteins in COS7 cells and examined their distribution. For additional comparisons, we also tested myosin X (MYO10) and myosin IIIa (MYO3A) in a similar assay. MYO10 possesses one MyTH4-FERM domain and MYO3A is a stereocilia myosin with no MyTH4-FERM domain (26). There was very limited, if any, colocalization of these myosins with the sans:harmonin-b plaques, as demonstrated by the much lower values of R and Rr compared with the values obtained for MYO7A (Fig. 4). MYO15A, MYO10, and MYO3A are known to transport cargo along COS7 filopodia (27, 28); however, they failed to transport harmonin-b or sans to filopodia tips (Fig. 4 *E*–*G*), suggesting specificity in the MYO7A MyTH4-FERM interactions with sans and harmonin-b. Next, we tested the interactions of MYO7A, sans, and harmonin-b in double-transfection combinations of these proteins in COS7 cells. Our results showed strong colocalization in each double transfection in each combination, independent of the third partner of the putative tripartite complex (Fig. S4). Association of the cluster with actin filament bundles occurred only when harmonin was present (Fig. S4). Interestingly, whirlin, which has been reported to bind sans in vitro (24), did not show significant colocalization with sans in our COS7 coexpression assay (Fig. S4).

UTLD Is Disrupted in a Harmonin-Mutant Mouse but Preserved in a MYO7A-Mutant Mouse. It has been shown that in harmonin-mutant *deaf circler (Ush1c$^{dfcr/J}$)* mice, harmonin clusters are largely dispersed along stereocilia with some accumulation at the stereocilia tips (13). These mice carry an in-frame large genomic deletion that encompasses exons encoding the domains required for actin binding (12, 13). We examined the distributions of MYO7A and sans in the postnatal day 13 *dfcr* mice, and compared these to the distribution of harmonin. The pattern of localization of MYO7A was very similar to harmonin, showing residual fluorescence puncta at the UTLD and accumulation at the stereocilia tips (Fig. S5). A similar pattern was observed for CDH23 immunofluorescence (Fig. S5). However, we could only rarely detect sans labeling at the UTLD and at the stereocilia tips in these mice. *Shaker-1* mutant mice carry a substitution in the motor head domain of MYO7A that is predicted to alter its motor activity; however, the protein expression level is virtually normal (29). We examined the distribution of UTLD components in postnatal day 13 *Shaker-1* mice. The outer hair-cell stereocilia showed the characteristic V-shaped organization with only two height-ranked rows of stereocilia instead of the typical three rows (Fig. S5). Immunofluorescence for MYO7A, sans, and harmonin showed that despite the MYO7A mutation all three proteins cluster at the UTLD (Fig. S5).

Disruption of Tip-Links Causes No Detectable Disruption or Movement of the UTLD. It is well established that reduction of Ca^{2+} concentration in the extracellular medium using the strong Ca^{2+} chelating agent BAPTA [1,2-bis(*o*-aminophenoxy) ethane-*N*,*N*,*N*′,*N*′-tetraacetic acid] causes tip-link disruption and loss of MET. However, it is not known what happens to the UTLD components when the tip-link is disrupted with BAPTA. One possibility is that the UTLD climbs upwards toward the stereocilia tip because of the action of the putative UTLD motor. Another possibility is that the UTLD plaque disassembles and reorganizes later when the tip-link is reformed. A previous report (4) showed that when hair cells were incubated for 1 min in 5 mM BAPTA and allowed to recover for 10 min at 37 °C, the CDH23 fluorescent puncta remained intact. To examine if the components of the UTLD remain in place after tip-link disruption, we labeled rat hair cells for MYO7A, harmonin, sans, and CDH23 following BAPTA treatment (Fig. S5). We did not detect changes in the labeling pattern for the three UTLD proteins, indicating that under the conditions of our BAPTA treatment experiment, despite the disruption of the tip-link, the UTLD maintains its overall integrity, and if there is any upwards movement it is of very limited extent (30).

Discussion

We used immunofluorescence and hair-cell transfections with tagged cDNA constructs to show that MYO7A and its binding partner sans are enriched at the UTLD (Fig. 5). A cluster of myosin motors at the UTLD is presumed to pull on the tip-link, producing a dynamic resting tension on the MET channel (1, 2, 6). An earlier study on MET properties in the *Myo7a^{6J}* and *Myo7a^{4626SB}* mouse mutants, which carry a R241P substitution in the motor head and a Q720X truncating mutation, showed that the normal resting current is abolished and the extent of adaptation is increased, suggesting that the tip-links are slack at rest (11). These results, in combination with our observation that MYO7A is clustered at the UTLD, strongly suggest that the MYO7A is the motor that tenses the tip-link. Moreover, if an individual myosin molecule produces a force around 1 to 2 pN (31, 32), then our estimation of ∼eight (varying from ∼5–12) MYO7A at the UTLD based on the immunofluorescence intensity is compatible with the ∼8 pN force presumed to be generated by the motor element at the UTLD (33).

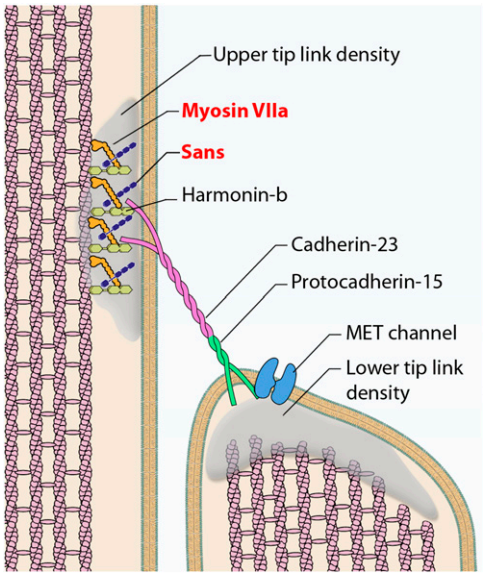

Fig. 5. Diagram of the mechanotransduction complex illustrating the localization of MYO7A and sans at the upper tip-link density. MYO7A localization is consistent with a role in tip-link tensing.

The motor for tip-link tensing has been naturally associated with the putative MET adaptation complex at the UTLD. MYO1C has been suggested as the MET adaptation motor based on early reports showing localization of MYO1C at both the upper and lower tip-link densities (7, 8) and on chemical-genetic studies where a Y61G mutation in MYO1C renders the molecule sensitive to NMB-ADP (9, 34). However, a more recent study showed MYO1C broadly distributed along the length of stereocilia (10), making it difficult to be certain of its localization and of its potential role at the UTLD. Furthermore, the studies using the Y61G mutation leave open the role of MYO1C in maintaining tip-link tension. The reported changes in resting tension, activation rise time, and adaptation produced when applying NMB-ADP to Y61G hair cells are not as great as expected from the effect of NMB-ADP on Y61G MYO1C in the in vitro assays. It is therefore possible that MYO7A is involved in maintaining a resting tension on the tip-link and the putative adaptation would be supported by MYO1C or other molecular components of the tip-link complex.

In addition to a motor, the UTLD is presumed to contain a mechanism that enables and controls slippage as part of the adaptation process. It has been shown that the tip-link can sustain at least 4 to 13 pN of tension, in addition to the ~8 pN of resting tension, when force is exerted on the stereocilia bundle (33). This additional regulated resistance to force can be provided by changes in the rigor state of the myosin and by the local modulation of the scaffolding properties of harmonin and sans. Harmonin has been proposed to mediate mechanical coupling between the tip-link and the stereocilia actin core (13). Two recent studies show that the kinetics of MET are altered when harmonin is mutated or missing (13, 22). It was inferred then that harmonin-b is an intracellular link that contributes to establishing MET channel sensitivity to displacement by limiting adaptation and engaging adaptation motors, a dual role consistent with its scaffolding property and its ability to bind to actin filaments and to the tip-link protein CDH23 (2, 13). Although harmonin is able to independently associate with actin and form plaques, our results show that sans is another scaffolding protein enriched at the UTLD. Furthermore, because harmonin is required to cluster sans and MYO7A, disruption of harmonin is likely to influence the role of sans and MYO7A at the UTLD. In fact, in the harmonin mutant *dfcr* mice, MYO7A migrates to the stereocilia tips together with CDH23 and sans is no longer detectable in stereocilia. The mutual dependence of these proteins for proper localization makes it difficult to evaluate the direct contribution of each one separately in MET function.

Our hair cell and COS7 cell transfection data show that MYO7A, sans, and harmonin-b form a tripartite complex and can also bind to each other independently. Our cursory attempts at estimating copy numbers from the relative fluorescence intensities indicate that MYO7A and sans are present at approximately the same number and that harmonin is present in higher copy numbers than MYO7A and sans. The relationship we found was ~8:9:23 for MYO7A, sans, and harmonin, respectively. Each of these proteins has multiple interacting domains that can contribute to formation of a very compact and stable complex. The presence of multiple copies of MYO7A and sans introduces the possibility of additional interactions at the UTLD. For example, the sans central (CEN) domain can bind to the N-terminal MyTH4-FERM module of MYO7A (14, 15), and the sans SAM-PBD domain can bind to the harmonin PDZ1 (35) and PDZ3 (15). In addition, MYO7A C-terminal MyTH4-FERM domain can bind to harmonin PDZ1 (12). This multitude of interactions is likely to result in a very stable structure (Fig. 5) that underlies the compact, electron-dense appearance of the UTLD in thin section electron microscopy.

A large number of Usher syndrome missense mutations occur in amino acids of the MYO7A MyTH4-FERM domains (http://www.hgmd.cf.ac.uk/ac/index.php). A recent crystal structure study examined the MYO7A MyTH4-FERM domain in complex with the sans CEN1 and -2 modules (14) and proposed that the binding depends on properties that are general to MyTH4-FERM domains. However, our results showing the inability or inefficiency of MyTH4-FERM domain-containing MYO15A and MYO10 to bind sans or harmonin point to an unidentified specificity of the MyTH4-FERM modules of MYO7A. Sequence analysis of MyTH4-FERM supramodules from MYO7A, MYO15A, and MYO10 show that their sequences can be aligned with high confidence (Fig. S6), but that the overall amino acid sequence identity of these domains is less than 10%. Sequence divergence between distinct modules is likely to confer specificity of binding and selectivity of localization and function. This finding could explain why, for example, MYO7A and MYO15A show quite distinct localization and function in the stereocilia, despite the fact that both of these motor proteins contain two MyTH4-FERM domains in their tails (25, 27).

Slow adaptation is thought to depend in large part on the movement of the upper tip-link insertion point. Previous studies have suggested that there is a limited extent of adaptation observed at the level of the receptor current (36) and limited movement of the UTLD has been observed in a preliminary electron microscopy study (30). Also, immunolocalization of CDH23, following disruption of the CDH23-PCDH15 tip-link with Ca^{2+} depletion and recovery for 15 min at 37 °C, showed limited ascent, if any, of CDH23 toward the stereocilia tip (4). We performed the same assay and followed the localization of CDH23, MYO7A, sans, and harmonin. We observed no evidence for changes in location or intensity of the labeling for any of these proteins. These results suggest that the UTLD is relatively stable and exhibits limited mobility (30), if any at all. It has been reported that tip-links can reform when bundles are allowed to recover from BAPTA treatment for periods of 12 to 24 h (37). Strikingly, in these experiments, adaptation does not recover fully even after 24 h (37). Little is known about the molecular rearrangements that precede the reformation of tip-links. If disassembly and reassembly of the UTLD is required, then the time-frame for these processes is likely to be in the range of hours or even days.

The colocalization of MYO7A, sans, harmonin, and CDH23 at the UTLD further supports the functional relevance of their

interactions and roles in causing hearing loss in USH1 syndrome. An understanding of how these proteins cooperate at early stages of bundle formation and MET assembly is necessary to better evaluate the processes underlying the disruption of stereocilia bundles in the early onset of deafness in USH1. For example, hair cells from the harmonin-deficient *deaf circler* mice showed dispersion of UTLD components, with CDH23 and the mutant harmonin migrating to stereocilia tips (13). However, in the *shaker-1* mice where MYO7A has a mutation in the motor domain that is predicted to limit its function (38), harmonin, sans, and MYO7A are still able to assemble at the UTLD. Previous reports suggested that MYO7A transports cargo to shorter stereocilia tips (39) and to the UTLD site (2). Although our results do not exclude the possibility that MYO7A serves as a stereocilia cargo transporter, the pattern of localization is more consistent with a role at the UTLD site. Our results, taken together with previous physiology data (11), suggest that, contrary to harmonin, functional MYO7A is not essential for the formation of the UTLD but is required for tip-link tensing. Another potential role for MYO7A and sans at the UTLD would be in the maintenance of stereocilia structure. Tension on the tip-link exerted from its UTLD could also influence the shape and length of the adjacent shorter stereocilia (40). At the tip-link lower insertion site, MET and actin regulation coexist (Fig. 5) and probably share molecular components (41). Thus, the reciprocal relationship between tip-link tension and actin dynamics could help regulate stereocilia length. Reduced tip-link tension as a result of mutations in MYO7A or other UTLD proteins could not only disrupt MET, but also cause shorter stereocilia (42) or even loss of stereocilia, as is the case for the *shaker-1* mouse where the outer hair cells show only two rows of stereocilia.

Materials and Methods

For a description of the materials and methods used for antibodies, Western blotting, immunocytochemistry, cDNA expression vectors, cultures, and transfection of rat inner-ear tissue, culture and transfection of COS7 cells, BAPTA treatment for tip-link disruption, mutant mice, and genotyping, and scanning electron microscopy, see *SI Materials and Methods*. Animal use was performed according to National Institutes of Health (NIH) guidelines under protocol approved by the Animal Care and Use Committee. Fluorescence quantification and image analysis were performed using ImageJ software (NIH).

ACKNOWLEDGMENTS. We thank Drs. L. Andrade, F. Salles, S. Ebrahim, U. Manor, and Y. Dai for help with experiments and with the manuscript. This work was supported by the Intramural Program of the National Institute on Deafness and Other Communication Disorders-National Institutes of Health.

1. Grillet N, et al. (2009) The mechanotransduction machinery of hair cells. *Sci Signal* 2: pt5.
2. Gillespie PG, Müller U (2009) Mechanotransduction by hair cells: Models, molecules, and mechanisms. *Cell* 139:33–44.
3. Sakaguchi H, Tokita J, Müller U, Kachar B (2009) Tip links in hair cells: Molecular composition and role in hearing loss. *Curr Opin Otolaryngol Head Neck Surg* 17: 388–393.
4. Kazmierczak P, et al. (2007) Cadherin 23 and protocadherin 15 interact to form tip-link filaments in sensory hair cells. *Nature* 449:87–91.
5. Kachar B, Parakkal M, Kurc M, Zhao Y, Gillespie PG (2000) High-resolution structure of hair-cell tip links. *Proc Natl Acad Sci USA* 97:13336–13341.
6. Ricci AJ, Kachar B, Gale J, Van Netten SM (2006) Mechano-electrical transduction: New insights into old ideas. *J Membr Biol* 209:71–88.
7. Garcia JA, Yee AG, Gillespie PG, Corey DP (1998) Localization of myosin-Ibeta near both ends of tip links in frog saccular hair cells. *J Neurosci* 18:8637–8647.
8. Steyger PS, Gillespie PG, Baird RA (1998) Myosin Ibeta is located at tip link anchors in vestibular hair bundles. *J Neurosci* 18:4603–4615.
9. Holt JR, et al. (2002) A chemical-genetic strategy implicates myosin-1c in adaptation by hair cells. *Cell* 108:371–381.
10. Schneider ME, et al. (2006) A new compartment at stereocilia tips defined by spatial and temporal patterns of myosin IIIa expression. *J Neurosci* 26:10243–10252.
11. Kros CJ, et al. (2002) Reduced climbing and increased slipping adaptation in cochlear hair cells of mice with Myo7a mutations. *Nat Neurosci* 5:41–47.
12. Boëda B, et al. (2002) Myosin VIIa, harmonin and cadherin 23, three Usher I gene products that cooperate to shape the sensory hair cell bundle. *EMBO J* 21:6689–6699.
13. Grillet N, et al. (2009) Harmonin mutations cause mechanotransduction defects in cochlear hair cells. *Neuron* 62:375–387.
14. Wu L, Pan L, Wei Z, Zhang M (2011) Structure of MyTH4-FERM domains in myosin VIIa tail bound to cargo. *Science* 331:757–760.
15. Adato A, et al. (2005) Interactions in the network of Usher syndrome type 1 proteins. *Hum Mol Genet* 14:347–356.
16. Yan D, Liu XZ (2010) Genetics and pathological mechanisms of Usher syndrome. *J Hum Genet* 55:327–335.
17. Weil D, et al. (2003) Usher syndrome type I G (USH1G) is caused by mutations in the gene encoding SANS, a protein that associates with the USH1C protein, harmonin. *Hum Mol Genet* 12:463–471.
18. Caberlotto E, et al. (2011) Usher type 1G protein sans is a critical component of the tip-link complex, a structure controlling actin polymerization in stereocilia. *Proc Natl Acad Sci USA* 108:5825–5830.
19. Hasson T, et al. (1997) Unconventional myosins in inner-ear sensory epithelia. *J Cell Biol* 137:1287–1307.
20. Yang Y, et al. (2009) A FERM domain autoregulates *Drosophila* myosin 7a activity. *Proc Natl Acad Sci USA* 106:4189–4194.
21. Umeki N, et al. (2009) The tail binds to the head-neck domain, inhibiting ATPase activity of myosin VIIA. *Proc Natl Acad Sci USA* 106:8483–8488.
22. Michalski N, et al. (2009) Harmonin-b, an actin-binding scaffold protein, is involved in the adaptation of mechanoelectrical transduction by sensory hair cells. *Pflugers Arch* 459:115–130.
23. Zinchuk V, Zinchuk O (2008) Quantitative colocalization analysis of confocal fluorescence microscopy images. *Curr Protoc Cell Biol* Chapter 4:Unit 4:19.
24. Maerker T, et al. (2008) A novel Usher protein network at the periciliary reloading point between molecular transport machineries in vertebrate photoreceptor cells. *Hum Mol Genet* 17:71–86.
25. Anderson DW, et al. (2000) The motor and tail regions of myosin XV are critical for normal structure and function of auditory and vestibular hair cells. *Hum Mol Genet* 9: 1729–1738.
26. Berg JS, Derfler BH, Pennisi CM, Corey DP, Cheney RE (2000) Myosin-X, a novel myosin with pleckstrin homology domains, associates with regions of dynamic actin. *J Cell Sci* 113:3439–3451.
27. Manor U, et al. (2011) Regulation of stereocilia length by myosin XVa and whirlin depends on the actin-regulatory protein Eps8. *Curr Biol* 21:167–172.
28. Salles FT, et al. (2009) Myosin IIIa boosts elongation of stereocilia by transporting espin 1 to the plus ends of actin filaments. *Nat Cell Biol* 11:443–450.
29. Mburu P, et al. (1997) Mutation analysis of the mouse myosin VIIA deafness gene. *Genes Funct* 1:191–203.
30. Shepherd GMG, Assad JA, Parakkel M, Kachar B, Corey DP (1991) Movement of the tip-link attachment is correlated with adaptation in bullfrog saccular hair-cells. *J Gen Physiol* 98:A25.
31. Huxley AF, Simmons RM (1971) Proposed mechanism of force generation in striated muscle. *Nature* 233:533–538.
32. Chuan P, Spudich JA, Dunn AR (2011) Robust mechanosensing and tension generation by myosin VI. *J Mol Biol* 405:105–112.
33. Jaramillo F, Hudspeth AJ (1993) Displacement-clamp measurement of the forces exerted by gating springs in the hair bundle. *Proc Natl Acad Sci USA* 90:1330–1334.
34. Stauffer EA, et al. (2005) Fast adaptation in vestibular hair cells requires myosin-1c activity. *Neuron* 47:541–553.
35. Yan J, Pan L, Chen X, Wu L, Zhang M (2010) The structure of the harmonin/sans complex reveals an unexpected interaction mode of the two Usher syndrome proteins. *Proc Natl Acad Sci USA* 107:4040–4045.
36. Shepherd GM, Corey DP (1994) The extent of adaptation in bullfrog saccular hair cells. *J Neurosci* 14:6217–6229.
37. Zhao Y, Yamoah EN, Gillespie PG (1996) Regeneration of broken tip links and restoration of mechanical transduction in hair cells. *Proc Natl Acad Sci USA* 93: 15469–15474.
38. Gibson F, et al. (1995) A type VII myosin encoded by the mouse deafness gene shaker-1. *Nature* 374:62–64.
39. Rzadzinska AK, Nevalainen EM, Prosser HM, Lappalainen P, Steel KP (2009) MyosinVIIa interacts with Twinfilin-2 at the tips of mechanosensory stereocilia in the inner ear. *PLoS ONE* 4:e7097.
40. Rzadzinska AK, Schneider ME, Davies C, Riordan GP, Kachar B (2004) An actin molecular treadmill and myosins maintain stereocilia functional architecture and self-renewal. *J Cell Biol* 164:887–897.
41. Manor U, Kachar B (2008) Dynamic length regulation of sensory stereocilia. *Semin Cell Dev Biol* 19:502–510.
42. Lefèvre G, et al. (2008) A core cochlear phenotype in USH1 mouse mutants implicates fibrous links of the hair bundle in its cohesion, orientation and differential growth. *Development* 135:1427–1437.